Infrared Spectroscopy of Phenol−$(H_2O)_{n>10}$: Structural Strains in Hydrogen Bond Networks of Neutral Water Clusters

Kenta Mizuse, Toru Hamashima, and Asuka Fujii*

Department of Chemistry, Graduate School of Science, Tohoku University, Sendai 980-8578, Japan

Received: June 30, 2009; Revised Manuscript Received: August 25, 2009

To investigate hydrogen bond network structures of tens of water molecules, we report infrared spectra of moderately size (n)-selected phenol−$(H_2O)_n$ ($\sim 10 \leq n \leq \sim 50$), which have essentially the same network structures as $(H_2O)_{n+1}$. The phenyl group in phenol−$(H_2O)_n$ allows us to apply photoionization-based size selection and infrared-ultraviolet double resonance spectroscopy. The spectra show a clear low-frequency shift of the free OH stretching band with increasing n. Detailed analyses with density functional theory calculations indicate that this shift is accounted for by the hydrogen bond network development from highly strained ones in the small ($n < \sim 10$) clusters to more relaxed ones in the larger clusters, in addition to the cooperativity of hydrogen bonds.

1. Introduction

Water is one of the most ubiquitous materials on the earth and it plays essential roles in the various chemical, biological, and geophysical processes.[1,2] Because the hydrogen bond governs the characteristic nature of water, the hydrogen bond network structure of water has been of broad interest. To understand the network structure of water at the molecular level, water clusters, $(H_2O)_n$, have been extensively studied both experimentally and theoretically.[3−55] Water clusters in the gas phase, isolated molecular systems consisting of a finite number of molecules, are expected to bridge the gap between the water monomer and bulk water by forming the most favored network structures, which depend on the cluster size (n).

The hydrogen bond network structures of the small-sized $(H_2O)_n$ clusters ($n \leq 10$) have been established by size-selected infrared (IR) and far-IR spectroscopy and theoretical calculations. A water dimer ($n = 2$) forms a linear structure,[3,10] and a ring structure starts to be formed at $n = 3$.[6,7] The water network develops to three-dimensional (3-D) structures such as cages at $n = 6$.[8] Characteristic cubes, which consist of six 4-membered rings, are identified at $n = 8$.[9,10,52,53] In this size region, the observed 3-D networks are dominated by the 4-membered ring motif, which consists of highly distorted hydrogen bonds. This makes a sharp contrast with the dominance of the 5- and 6-membered ring motifs in clathrate hydrates or hexagonal ice (Ih), which are examples of the bulk water structures.[1−3]

For larger clusters ($n > \sim 10$), Page et al. measured IR spectra of moderately size-selected $(H_2O)_n$ ($n \sim 19$) using electron ionization mass spectrometry for the size selection;[5] however, no specific structures were discussed. Except for this work, only IR spectra of the mean size ($\langle n \rangle$)-controlled water clusters ($\sim 20 \leq \langle n \rangle \leq \sim 1\,000\,000$) have been reported.[4,13−15] These spectra have shown that the low-frequency shift of the broadened hydrogen-bonded OH stretch band evidences the network development from "amorphous" to "crystal interior" ($n > 200-1000$).

On the other hand, extensive theoretical studies for the $n = \sim 10$ to ~ 50 clusters have indicated that the 4-membered ring motif becomes less important with increasing cluster size while the 5- and 6-membered ring motifs become superior.[4,16−30] However, previously reported IR spectra suffer from widely distributed sizes,[4,13−15] low spectral resolution,[4,5,15] and/or contaminant adsorption.[4] Then, correlations between detailed cluster structures and IR spectral features have not been examined in this size region.

To analyze hydrogen bond network structures consisting of tens of water molecules, we report here IR spectra of the chromophore-labeled water clusters, phenol−$(H_2O)_n$ ($\sim 10 \leq n \leq \sim 50$). Phenol−$(H_2O)_n$ has the advantage of having an ultraviolet (UV) chromophore (the phenyl ring), which enables us to apply various spectroscopic techniques based on the UV electronic transition. Phenol−$(H_2O)_n$ has been studied extensively by, for example, fluorescence excitation, resonant two-photon ionization, and various double resonance spectroscopies.[36−50] These studies, especially vibrational spectroscopy (IR−UV double resonance spectroscopy) in the OH stretch region,[43,45,46,49,50] showed that phenol−$(H_2O)_n$ are structural analogues of neat $(H_2O)_{n+1}$ because the hydroxy group of the phenol plays a compatible role as that of a water in the hydrogen bond network. For phenol−$(H_2O)_n$[43,45,46,49,50] and the similar system, benzene−$(H_2O)_{n+1}$,[51−54] size-selected IR spectra have been measured up to $n \leq 8$ using their size-specific UV transitions. These IR spectroscopic studies on chromophore-labeled water clusters have pioneered structural studies on small-sized water networks as those of neat $(H_2O)_n$ clusters[6−10] have done.

For larger-sized clusters ($n > \sim 10$) with a chromophore, UV absorption bands are generally broadened and IR−UV double resonance spectroscopy has been considered useless for the size selection. In this study, however, we use the scheme of the IR−UV double resonance but utilize only photoionization mass spectrometry to select the cluster size. Though we sacrifice the rigorous size selection because of the fragmentation upon ionization, we still achieve moderate size selectivity ($0 \leq \Delta n \leq 6$, see the Experimental Section) in the IR spectral measurement of phenol−$(H_2O)_n$ by monitoring the $[\text{phenol}-(H_2O)_n]^+$ ion signal.

In this study, to probe detailed network structures, we focus on the free (dangling) OH stretching band. Chang and coworkers have reported that a free OH stretching frequency of

* To whom correspondence should be addressed. E-mail: asukafujii@mail.tains.tohoku.ac.jp.

10.1021/jp9061187 CCC: $40.75
Published on Web 09/28/2009

water clusters is more sensitive to surrounding hydrogen bond environments, e.g., coordination numbers and hydrogen bond directionalities.[55,56] In contrast, hydrogen-bonded OH stretch bands are broadened in the large-sized clusters and are difficult to analyze.[5] Analyses of free OH bands actually have played key roles in the structure studies on cationic hydrated clusters.[55−60] However, no serious analysis of free OH frequencies has been performed for medium- to large-sized ($n > \sim 10$) neutral water clusters. Here, we demonstrate that the free OH stretching frequency of phenol−$(H_2O)_n$ shows a low-frequency shift with increasing cluster size. The observed shift is accounted for by the hydrogen bond network development of water clusters from the highly strained 4-membered ring motif to the more relaxed 5- and 6-membered ring motifs as well as by the cooperativity of hydrogen bonds.

2. Experimental Section

2.1. Infrared Spectroscopy. The gas phase phenol−$(H_2O)_n$ clusters were produced in a pulsed supersonic jet expansion of the gaseous phenol/water mixture diluted with helium. IR spectra of moderately size-selected phenol−$(H_2O)_n$ ($n = 11-49$) in the free OH stretch region (3650−3750 cm^{-1}) were measured by the IR−UV double resonance technique combined with mass spectrometry. The [phenol−$(H_2O)_n$]$^+$ ions produced by one-color resonant two-photon ionization (R2PI) of neutral clusters were mass-selected by a time-of-flight mass spectrometer. Because of the fragmentation upon ionization, [phenol−$(H_2O)_n$]$^+$ ions can be produced by R2PI of phenol−$(H_2O)_{n+\Delta n}$ (Δn is the number of evaporated water molecules upon ionization). As we will discuss later, the maximum Δn upon one-color R2PI is evaluated to be 6 or less. Then, the [phenol−$(H_2O)_n$]$^+$ ion intensity can be a measure of the ground state population of phenol−$(H_2O)_{n+\Delta n}$ ($0 \le \Delta n \le 6$). An application of two-color R2PI spectroscopy with an ionization UV pulse at a suitable frequency should reduce the excess energy and suppress fragmentation upon ionization. Though we actually applied the two-color R2PI scheme for the present large-sized clusters, the two-color ionization signal was hardly detected. This is because the production yields of the large-sized clusters are so low that we need to use a relatively intense UV pulse for the first electronic excitation, and it significantly reduces the ionization by the second UV pulse.

Figure 1 shows the one-color R2PI spectra of phenol−$(H_2O)_n$ obtained by monitoring [phenol−$(H_2O)_n$]$^+$. Only a structureless absorption band is seen in Figure 1 for $n \ge 9$. The maximum size of the cluster which shows sharp vibronic bands has been reported to be $n = 12$ (by two-color R2PI spectroscopy).[48,49] Contribution of larger clusters due to fragmentation and inherent broadening in large-sized clusters would wash out sharp spectral features in the present spectra. The UV frequency was tuned to 36254 cm^{-1}, which is near the maximum of the broad absorption of large-sized clusters, and the [phenol−$(H_2O)_n$]$^+$ ion intensity was monitored. Then, an IR pulse was introduced prior to the UV pulse and its frequency was scanned. When an IR transition occurs in phenol−$(H_2O)_{n+\Delta n}$, the monitored [phenol−$(H_2O)_n$]$^+$ signal decreases because of the vibrational predissociation of the clusters.

Figure 2 shows the mass distribution of [phenol−$(H_2O)_n$]$^+$ produced by R2PI in the IR spectral measurement condition for phenol−$(H_2O)_{49}$. The red curve in Figure 2 shows the mass distribution with the IR irradiation, while the black curve shows that without the IR irradiation. Figure 2 demonstrates that IR absorption causes predissociation of neutral clusters. The IR spectrum of the moderately size-selected cluster was measured as an ion-dip spectrum by monitoring the [phenol−$(H_2O)_n$]$^+$ ion intensity. Because IR predissociation of larger-sized clusters results in the fragmentation to the monitored ion channel [phenol−$(H_2O)_n$]$^+$, it causes an offset to the IR ion-dip spectrum of the cluster size of interest. To reduce such interference from larger-sized clusters, in every IR spectral measurement, we adjusted the cluster size distribution to reduce the clusters larger than that of interest by changing the jet expansion conditions. For example, the size distribution shown as the black curve in Figure 2 is optimized for the IR measurement of $n = 49$.

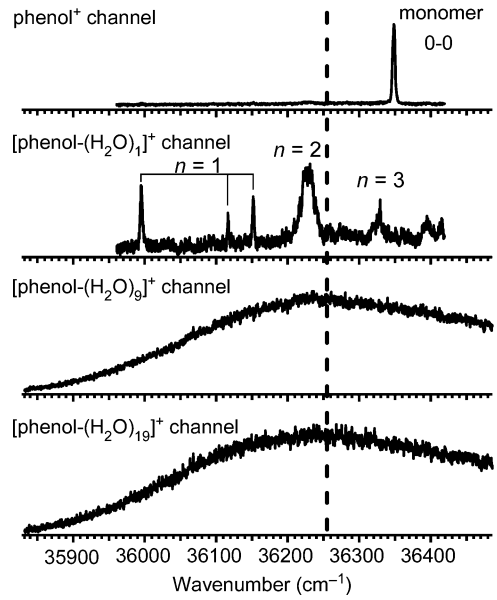

Figure 1. One-color resonant two-photon ionization spectra of phenol−$(H_2O)_n$ obtained by monitoring [phenol−$(H_2O)_n$]$^+$ ions. The assignments were taken from refs 38, 40, 41, 45, and 46. The dashed line indicates the UV photon energy, 36254 cm^{-1}, used for the photoionization in the IR spectral measurements.

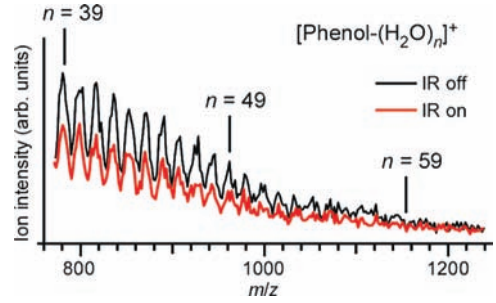

Figure 2. Mass distribution of [phenol−$(H_2O)_n$]$^+$ produced by R2PI. The condition of the cluster production was optimized for the IR spectral measurement of phenol−$(H_2O)_{49}$. The red curve shows the mass distribution with the IR irradiation, while the black one shows the distribution without the IR irradiation.

We should note that structural isomer selectivity is not achieved by the present IR spectroscopy. In a supersonic jet expansion, a number of energetically low-lying isomers would be formed especially for large-sized clusters, and we would observe an ensemble of such various structural isomers in the cluster size of interest. Moreover, there are many free OH oscillators in each cluster. The free OH frequency in this experiment was determined by the maximum of the single Lorentzian fitting of overlapped free OH bands. Therefore, the observed spectra should be regarded to reflect the averaged behavior of the water network structures in the ensemble of the clusters.

The experimental setup has been described elsewhere,[46] and only a brief description is given here. UV light was the second

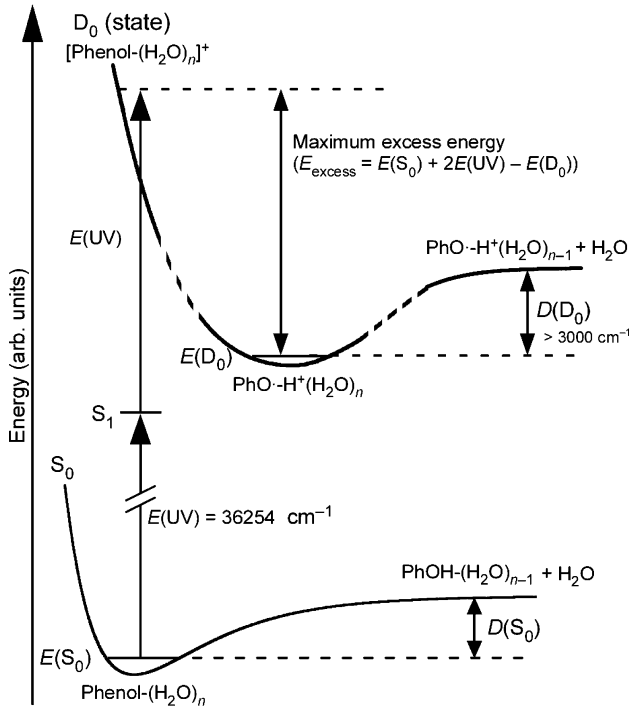

Figure 3. Schematic energy diagram on the photoionization and dissociation of phenol$-(H_2O)_n$.

harmonic of a dye laser output (Laser Analytical System LDL20505 with Coumarin 540A dye) pumped by a Nd:YAG laser (Continuum Surelite III). IR light was obtained by the difference frequency mixing with a $LiNbO_3$ crystal between the second harmonic of a Nd:YAG laser (Continuum Powerlite 8000) and an output of a dye laser (Continuum ND6000 with DCM and LDS698 dyes). The wavelength of the IR light was calibrated (in vacuum wavenumbers) by recording an ambient water vapor spectrum. All of the presented IR spectra were normalized by the IR power.

2.2. Size Selectivity. Because hydrogen-bonded clusters usually suffer from fragmentations in an ionization process, it is difficult to precisely measure the size distribution of the neutral clusters only from mass spectrometry. However, for phenol$-(H_2O)_n$, the number of evaporated water molecules (Δn) upon one-color R2PI can be estimated to be six or less by the energetics calculations. Figure 3 shows the schematic energy diagram on the photoionization and dissociation of phenol$-(H_2O)_n$. Because the one water loss channel ($[M\text{-}(H_2O)_n]^+ \rightarrow [M\text{-}(H_2O)_{n-1}]^+ + H_2O$) is the major dissociation path in cationic hydrated clusters with excess energies,[61] we assume the sequential evaporation of water one by one upon ionization. Then, the *maximum* Δn is evaluated by

$$\text{maximum } \Delta n = E_{\text{excess}}/D(D_0) \qquad (1)$$

where E_{excess} is the maximum excess energy upon ionizations and $D(D_0)$ is the dissociation energy of the one water loss channel in the cationic state. Because [phenol$-(H_2O)_n]^+$ ($n \geq 3$ or 4) forms an intracluster proton-transferred [PhO•$-H^+$-$(H_2O)_n$] type structure,[62−64] the values of $D(D_0)$ of $H^+(H_2O)_n$, which have been measured by the mass spectrometric technique,[65] can be used here. E_{excess} is given by

$$E_{\text{excess}} = 2E(\text{UV}) - [E(D_0) - E(S_0)] + D(S_0) \qquad (2)$$

where $E(S_0)$ and $E(D_0)$ are the absolute energies of phenol$-(H_2O)_n$ and [PhO•$-H^+(H_2O)_n$] at the zero-point level, respectively, then $[E(D_0) - E(S_0)]$ is the adiabatic ionization energy of the phenol$-(H_2O)_n$; E(UV) is the UV photon energy (36254 cm^{-1}), and $D(S_0)$ is the dissociation energy in the S_0 state. In eq 2, $D(S_0)$ accounts for the maximum internal energy of the phenol$-(H_2O)_n$. Though we employ the supersonic jet cooling technique, the clusters have finite internal energies (temperatures). In addition, broadened electronic spectra of the large-sized clusters prevent us from evaluating the internal energy. The maximum internal energy of the cluster should be lower than $D(S_0)$, because clusters with internal energy higher than $D(S_0)$ spontaneously dissociate into smaller-sized clusters prior to arrival at the interaction region with the lasers. With these relations, we examine the energetics of dissociation of phenol$-(H_2O)_{11,19}$ following the photoionization, as typical examples. $E(S_0)$ and $E(D_0)$ are evaluated using density functional theory (DFT) calculations at the B3LYP/6-31+G(d) level (see section 2.3). Calculated adiabatic ionization energies, $[E(D_0) - E(S_0)]$, are 56090 cm^{-1} for phenol$-(H_2O)_{11}$ and 54935 cm^{-1} for phenol$-(H_2O)_{19}$. For $H^+(H_2O)_{11,19}$, experimental $D(D_0)$ values are larger than 3000 cm^{-1}.[65] $D(S_0)$ is generally smaller than $D(D_0)$ because of the enhanced electrostatic interactions in the ionic state.[66] Then, from eqs 1 and 2, the *maximum* Δn is evaluated to be 6 in both cases. Cluster structures calculated for energy evaluation were shown in the Supporting Information.

2.3. Quantum Chemical Calculations. For the detailed analyses of the cluster structures and their correlations with free OH frequencies as well as their energies, DFT calculations were carried out using the B3LYP functional[67] with the 6-31+G(d) basis set. The initial geometries of $(H_2O)_n$ were obtained from the reported low-lying minima or characteristic structures;[19,24,25] otherwise, they were manually constructed. Those of phenol$-(H_2O)_{n-1}$ were constructed by substituting one of the free hydrogen atoms in $(H_2O)_n$ to the phenyl group. In the energetics calculations, the structures of [PhO•-$H^+(H_2O)_{11,19}$] were constructed by putting a PhO• radical on a free OH group of the global minimum structures of $H^+(H_2O)_{11,19}$,[68] which have been extensively studied experimentally and theoretically.[57−60,69,70] All of the cluster structures considered here were fully geometry-optimized.

At the stationary points, harmonic frequencies and IR intensities were calculated. All of the calculated frequencies were scaled by a single factor of 0.9736, which was determined to reproduce the free OH stretching frequency of the cubic water octamer. There have been three experimental reports on the free OH frequency of cubic water octamer, i.e., $(H_2O)_8$,[9,10] benzene$-(H_2O)_8$,[52,53] and phenol$-(H_2O)_7$.[49] Here, we employed the value of benzene$-(H_2O)_8$, 3713.5 cm^{-1},[52] as a reference experimental value to determine the scaling factor because of the following reasons: The previously reported spectrum of neat $(H_2O)_8$ suffers from low spectral resolution for precise determination of the free OH frequency.[9,10] On the other hand, the resolution in the spectra of benzene$-(H_2O)_8$ is high enough.[52,53] In addition, perturbation of the benzene ring on the free OH frequency is estimated to be negligible because free OH bands in both benzene$-(H_2O)_8$ and (benzene)$_2-(H_2O)_8$ show essentially the same frequency.[53] Though Kleinermanns and co-workers reported the free OH frequencies of 3711.5 cm^{-1} (D_{2d} type) and 3710.5 cm^{-1} (S_4 type) for cubic phenol$-(H_2O)_7$, they employed atmospheric wavenumbers for their calibration.[49,50] We confirm that their experimental values for phenol$-(H_2O)_7$ are in agreement with our calculated values, 3712.7 cm^{-1} (D_{2d} type) and 3712.1 cm^{-1} (S_4 type) at the B3LYP/6-31+G(d) level of theory

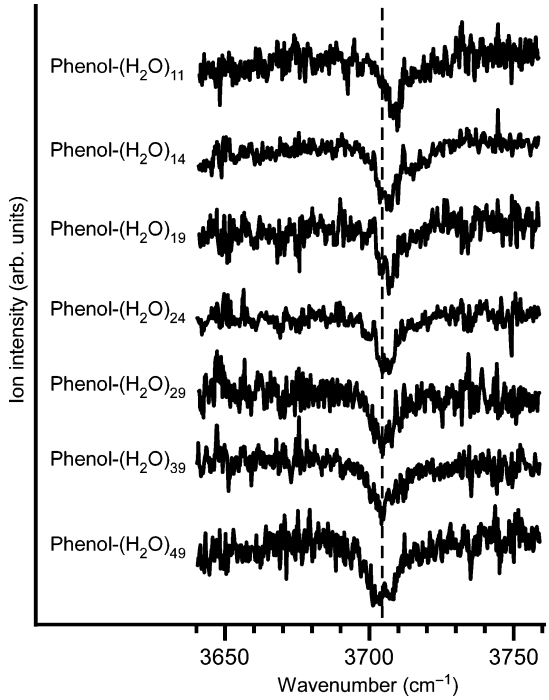

Figure 4. Moderately size-selected IR spectra of phenol−$(H_2O)_n$ (n = 11−49) in the free OH stretch region measured by monitoring $[phenol-(H_2O)_n]^+$. Each spectrum includes the contribution of larger-sized clusters of phenol−$(H_2O)_{n+\Delta n}$, where $0 \le \Delta n \le 6$. The dashed line is an eye guide.

with the scaling factor of 0.9736 when the vacuum correction (addition of ca. 0.8−1 cm^{-1} to atmospheric wavenumbers)[50] is included.

The calculated stick spectra were transformed into the continuous IR spectra by using a Lorentzian function with 10 cm^{-1} full width at half-maximum for each free OH stretching mode. The calculated free OH frequency reported in this study is the maximum of the single Lorentzian fitting of these overlapped multiple Lorentzian curves of the free OH bands. Then, we should note that we discuss the averaged behavior of the free OH bands. The present theoretical method has been used in the previous work on various hydrated clusters of the broad size range ($\sim 6 \le n \le \sim 30$) and has successfully reproduced experimental IR spectra with acceptable computational costs.[55,56,59] All of the energy values include zero-point corrections. All of the calculations in this study were carried out using the Gaussian 03 program.[71] The cluster structures were drawn with the MOLEKEL program.[72] Optimized structures of the clusters considered here are shown in the Supporting Information.

3. Results and Discussion

3.1. Observed Free OH Stretch Band of Phenol−$(H_2O)_n$. Figure 4 shows the IR spectra of phenol−$(H_2O)_n$ (n = 11−49) in the free OH stretch region measured by monitoring $[phenol-(H_2O)_n]^+$. Each spectrum includes the contribution of the larger-sized clusters of phenol−$(H_2O)_{n+\Delta n}$ ($0 \le \Delta n \le 6$). All of the spectra show a single band feature in this region. Since previous studies have revealed that $(H_2O)_{n\ge 6}$ clusters form 3-D structures consisting mainly of three-coordinated water molecules,[4,8−35,45−54] the band is assigned to the free OH stretching modes of such water molecules. Figure 4 shows a low-frequency shift of the band with increasing cluster size. Though this shift is somewhat slight, this is clear and reproducible. Observation of this shift demonstrates that the moderate size selection of the spectral carrier is achieved by using photoionization mass spectrometry. The observed free OH frequencies are summarized in Table 1. Compared to cubic $(H_2O)_8$, the magnitude of the shift amounts to 9 cm^{-1} in phenol−$(H_2O)_{49}$. We should note that the frequency shift observed in this study would lead to the similar one reported for the water nanoparticles in the much larger size range (n = $\sim 200-10^6$),[4] though the relation between the shift and hydrogen bond network structures has not been clarified so far.

TABLE 1: Observed Frequencies of the Free OH Stretching Bands in Phenol−$(H_2O)_{n+\Delta n}$ (n = 11−49)[a]

cluster	frequency (cm^{-1})	cluster	frequency (cm^{-1})
benzene−$(H_2O)_8$	3713.5	phenol−$(H_2O)_{24}$	3706.0
phenol−$(H_2O)_{11}$	3709.0	phenol−$(H_2O)_{29}$	3705.1
phenol−$(H_2O)_{14}$	3707.2	phenol−$(H_2O)_{39}$	3705.3
phenol−$(H_2O)_{19}$	3706.8	phenol−$(H_2O)_{49}$	3704.5

[a] These values are determined by the single Lorentzian fitting of the free OH bands. Each cluster size has the uncertainty of $0 \le \Delta n \le 6$. Errors in the frequencies are within ±1 cm^{-1}. The value of benzene−$(H_2O)_8$ is taken from ref 52.

A lower free OH frequency is generally expected when the surrounding hydrogen bonds are stronger. This is because the electron density on the free OH bond is slightly withdrawn by the neighboring proton donor molecules. Then, the observed low-frequency shifts show that the hydrogen bonds increase their mean strengths as the network grows. In the following, we discuss the origins of the enhancement of the hydrogen bond strengths.

3.2. Cooperative Effect in Water Clusters. One of the possible factors to explain the enhancement of the hydrogen bond strength is its cooperativity.[2,3] The cooperative effect essentially originates from the nonadditivity of the induction and dispersion terms. This effect means mutual enhancement among hydrogen bonds, and the magnitude of the effect increases with increasing number of surrounding hydrogen bonds. To evaluate the magnitude of the free OH frequency shifts caused by the cooperativity, we performed DFT calculations at the B3LYP/6-31+G(d) level. We calculated the free OH vibrational frequencies of the "fused-cube" type structures (see insets in Figure 5), which are designed to examine only the cooperative effect. These structures are an extension of cubic $(H_2O)_8$, increasing the number of hydrogen bonds while keeping the network motif, which consists only of the 4-membered rings. In Figure 5, filled circles show the observed free OH frequencies plotted versus the cluster sizes. The open circles and triangle in Figure 5 represent the calculated free OH frequencies for phenol−$(H_2O)_7$ and benzene−$(H_2O)_8$, respectively. These frequencies agree with the previously reported experimental values (see also the Experimental Section).[49,52] Open squares in Figure 5 show the calculated free OH frequencies of "fused-cube" clusters. Calculated frequencies of cubic $(H_2O)_n$ show the low-frequency shift similar to the experimental observations. However, the magnitude of the shifts in the "fused-cube" series is estimated to be much smaller than that in the experimentally observed series. These results suggest that the cooperativity accounts for only a part of the observed low-frequency shifts.

It has been pointed out that the B3LYP functional is unable to treat systems in which the dispersion interaction plays vital roles.[73] To evaluate the magnitude of the cooperative effect in interaction energy, the B3LYP functional may underestimate such interactions. Though many new functionals have recently been proposed for better inclusion of the dispersion interactions

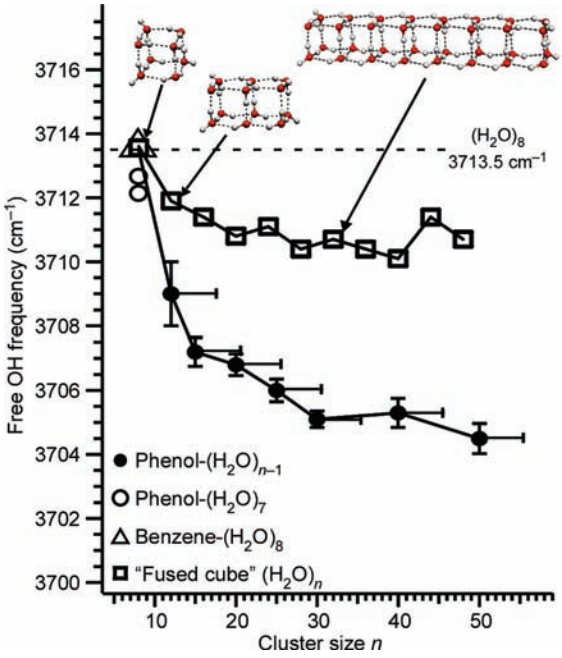

Figure 5. Size-dependent free OH frequencies of phenol−$(H_2O)_{n-1}$ observed by IR spectroscopy (filled circles) and those of "fused-cube" $(H_2O)_n$ obtained by calculations (open squares). Calculated values were obtained at the B3LYP/6-31+G(d) level, in which the harmonic frequencies were scaled by a factor of 0.9736. The insets show the "fused-cube" structures. The open circles and triangle show the calculated free OH frequencies for phenol−$(H_2O)_7$ and benzene−$(H_2O)_8$, respectively, which agree with the corresponding experimental values.[49,52]

and the long-range electron correlations,[74−80] evaluation of vibrational frequencies by these functionals is underway. As for frequency calculations (at least for scaled harmonic frequencies), the B3LYP functional with a suitable basis set seems to be the best-balanced method between the computational cost and accuracy for large-sized clusters. Furthermore, *ab initio* calculations for cubic $(H_2O)_8$ and $(H_2O)_{20}$ at the MP2/aug-cc-pVDZ level were reported by Xantheas and co-workers.[22,31] These high-level calculations, however, predict the low-frequency shift of ∼1 cm^{-1} from $(H_2O)_8$ to $(H_2O)_{20}$. This small shift suggests that the present DFT calculations do not significantly underestimate the frequency shift due to the cooperative effect.

3.3. Structural Strains in Water Clusters. Another possible factor for the low-frequency shifts of the free OH bands is the change of the hydrogen bond network structural motif, which also affects hydrogen bond strength. On the basis of the DFT calculations for the small-sized $(H_2O)_n$ ($n \leq 10$), Jiang et al. have shown the hydrogen bond distortion affects the free OH frequency.[55] To evaluate such a structural effect on the free OH frequency, we calculated model structures of larger-sized clusters. Figure 6 shows some characteristic model structures of $(H_2O)_{18-20}$[3,4,16−30] and those of corresponding phenol−$(H_2O)_{17-19}$ with the frequencies of the free OH bands simulated using DFT. Optimized cluster structures of four different types of networks are shown. The frequencies of phenol−$(H_2O)_{17-19}$ of the same hydrogen bond network are presented in parentheses, and they show the perturbation caused by the phenyl group is less than 1.5 cm^{-1} for the free OH frequency. Among these structures, the "fused-cube" consists only of 4-membered rings and has highly distorted hydrogen bonds, the same as cubic $(H_2O)_8$. The "prism" structure, which consists of 4- and 5-membered rings, has been predicted to be the energetically global minimum in $(H_2O)_{20}$ by the various theoretical studies including high-level *ab initio* calculations.[4,17−30] The "dodecahedral cage" consists of twelve 5-membered rings and can be regarded as the partial structure of clathrate hydrates.[2,3] "Hexagonal ice" has a very similar network structure to the crystalline hexagonal ice, consisting only of 6-membered rings. The distortions of hydrogen bonds in the "dodecahedral cage" and "hexagonal ice" structures are much less: the hydrogen bond angles are straighter (O−H···O angle is 170−180°) in the 5- and 6-membered rings than those in the 4-membered rings (O−H···O angle is 140−170°). Figure 6 shows the clear correlation between the magnitude of the hydrogen bond distortions and the free OH frequencies. The free OH frequency of the most strained "fused-cube" is predicted to be the highest value, 3710.8 cm^{-1} (3710.9 cm^{-1} in corresponding phenol−$(H_2O)_n$), and those of the less strained "dodecahedral cage" and "hexagonal ice" are 3704.2 cm^{-1} (3704.2 cm^{-1}) and 3702.7 cm^{-1} (3703.3 cm^{-1}), respectively. The free OH frequency of "prism" locates in between those of "fused-cube" and "dodecahedral cage" (or "hexagonal ice"), reflecting the coexistence of the 4- and 5-membered ring motifs. It should be noted that the frequency calculations at the MP2/aug-cc-pVDZ level also show a similar correlation.

The experimental frequency of phenol−$(H_2O)_{19}$ is located between "prism" and "dodecahedral". This location suggests the observed water networks of $n \sim 20$ consist not only of 4-membered rings but also of 5- and/or 6-membered rings. At this time, the 4-membered ring motif is no longer exclusive and the networks are being replaced by more relaxed structural motifs.

For further confirmation, similar analyses were carried out for the larger clusters. Figure 7 shows characteristic structures and their free OH frequencies of $(H_2O)_{48}$.[19] The values of corresponding phenol−$(H_2O)_{47}$ are also shown in the parentheses. These calculations show the same trend as $(H_2O)_{20}$. The free OH frequency of the most strained "fused-cube" structure is evaluated to be the highest, while those of the more relaxed "hexagonal prism" and "filled cage" are evaluated to be lower. As is in $(H_2O)_{18-20}$, the frequency of the "fused-cube" is much higher than the experimental value, meaning that the 4-membered ring (cubic) motif is not exclusive in the hydrogen bond network. In the case of $(H_2O)_{20}$ in Figure 6, the frequency of the "prism" structure is nearest to the experimental value. On the other hand, the free OH frequency of "hexagonal prism" in $(H_2O)_{48}$ no longer agrees with the experimental value, while the more relaxed "filled cage", which is the reported global minimum on the TIP4P potential energy surface,[19] is in good agreement with the observation. The contribution of the 4-membered rings in this "filled cage" was reported to be only 18%, and the 5- and 6-membered rings are clearly dominant.[19]

These results indicate that the hydrogen bond network structure develops from the highly strained 4-membered ring motif to the more relaxed motifs of 5- and 6-membered rings with the growth of the network, and the low-frequency shift of the free OH stretching band originates from the gradual transition of the structural motifs as well as the hydrogen bond cooperativity. This interpretation is consistent with the structural trends of hydrogen bond network development, which have been predicted by theoretical calculations. At $n = 8$, the 4-membered rings are exclusive (100%). With increasing size, at $n \sim 20$, the contributions of the 5- or 6-membered rings become necessary to reproduce the experimental frequency (in the plausible "prism" structure, the 4-membered rings still take over

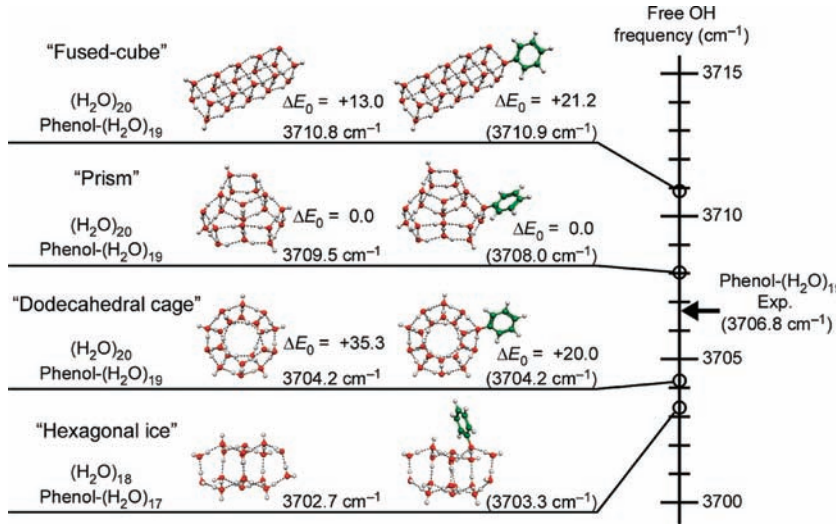

Figure 6. Free OH stretching frequencies of the characteristic cluster structures of $(H_2O)_{18-20}$ and corresponding phenol−$(H_2O)_{17-19}$. For $(H_2O)_{20}$ and phenol−$(H_2O)_{19}$, the relative energies at the vibrational zero-point level (ΔE_0) were also shown in kJ/mol. All of the cluster structures, their harmonic frequencies, and relative energies were calculated at the B3LYP/6-31+G(d) level. The harmonic frequencies were scaled by a factor of 0.9736. In "hexagonal ice", the free OH stretching modes of the two-coordinated water molecules and the π-hydrogen-bonded OH bond were excluded from the evaluation of the free OH frequency.

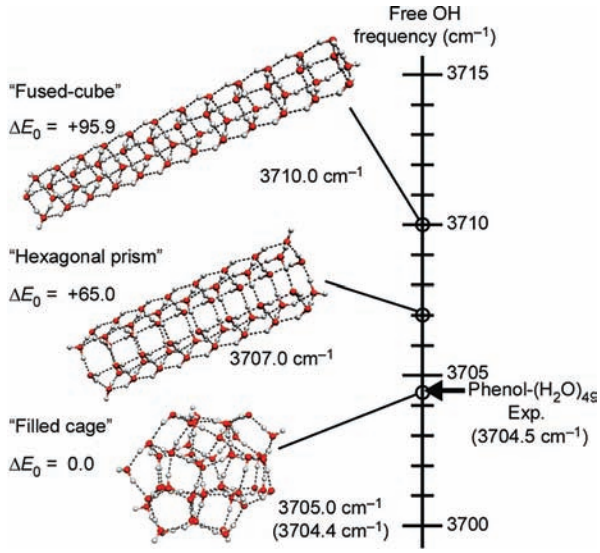

Figure 7. Free OH stretching frequencies and the relative energies (ΔE_0) in kJ/mol of the characteristic cluster structures of $(H_2O)_{48}$. The frequencies of corresponding phenol−$(H_2O)_{47}$ were also shown in parentheses. Each cluster structure and its energy and harmonic frequencies were calculated at the B3LYP/6-31+G(d) level, and all of the harmonic frequencies were scaled by a factor of 0.9736.

67% of the network). Then, at $n \sim 50$, the contribution of the 4-membered rings is estimated to be ~20%.

Because the experimental and calculated free OH frequency shifts are somewhat slight (within 10 cm^{-1}), accuracy of the calculated frequencies is critical. Actually, the absolute accuracy of the scaled harmonic frequencies based on the B3LYP/6-31+G(d) level has been estimated to be only ~20 cm^{-1}.[81] However, we optimized the scaling factor for free OH stretching frequencies and essentially focused on the relative frequencies. Then, the reliability of the present calculations will be higher. Furthermore, the MP2/aug-cc-pVDZ level calculations of $(H_2O)_{20}$ also show a similar correlation between the hydrogen bond distortions and the free OH frequencies.[22] The consistency of these higher-level calculations and our DFT calculations suggests that such correlation is a general trend and that the experimental frequency shift, more or less, is accounted for by the relaxation of the hydrogen bond distortions. Of course, further discussion will be done by fine anharmonic frequency calculations, which will be available in the near future.

In addition to the effect of the hydrogen bond distortion, Jiang et al. have reported another factor for the free OH frequency shift.[55] On the basis of the DFT calculations for model clusters, they showed that neighboring four-coordinated waters lower the free OH frequency relative to neighboring three-coordinated waters.[55] The present calculations are helpful to estimate the magnitude of such a coordination environment effect in the larger-sized region. In Figure 6, the free OH bond in the "dodecahedral cage" is surrounded by three three-coordinated waters and that in the "fused-cube" is surrounded by two three-coordinated and one four-coordinated waters. However, the free OH frequency in the "fused-cube" is calculated to be higher than that in the "dodecahedral cage". These calculations suggest that the network distortion is more effective than the neighboring water coordination effect in the size region of $n \sim 20$.

In the present DFT analyses, we pick up some characteristic cluster structures to examine the correlation between the structural strain and the free OH frequency. However, it should be noted that numerous structural isomers exist in the observed sizes, and only their averaged trend associated with the size is reflected in the observed frequency. No specific isomer structures can be identified in the present study, but only the general trend in the network development is inferred. Though the present calculations show the clear correlation between the observed frequency shift and the structural strain in the water network, extensive sampling of isomer structures or global search of potential energy surfaces[32,33] is requested for unequivocal proof of the origin of the shift. Such calculations for clusters of $n >$ ~10 are very time-consuming, and are beyond the scope of the present study.

Finally, we comment on the effect of the cluster temperature. Finite (and undefined) temperature or internal energy of clusters affects their preferential structures.[11,12,33−35] In conventional IR−UV double resonance spectroscopy of a jet-cooled neutral cluster, only a few energetically low-lying isomers are ordinarily considered because low temperature (or specific internal energy) of the cluster can be ensured by sharp vibronic bands in its electronic spectrum.[45,46,49,50,52−54] In the present experiment,

broadened electronic spectra of the large-sized clusters prevent us from evaluating the cluster temperature. In addition, the optimization of the size distribution in each IR measurement might cause the size dependence of the temperature of the observed clusters. Though the temperature of the clusters is an ambiguous factor in the present experiment, we infer that the size dependence of the cluster temperature is not a major origin of the observed OH frequency shift because of the following reasons: (i) The observed shift is reproducible irrespective of arbitrary optimization of the jet condition and size distribution. (ii) For both $(H_2O)_{20}$ and $(H_2O)_{48}$, the calculated free OH frequencies based on the reported energetically global minimum structures are in agreement with the experimental values. These agreements imply the observed IR spectra of both $n \sim 20$ and ~ 50 reflect low-lying cluster structures. (iii) The similar low-frequency shift has been found for ice nanoparticles of the much larger size range ($n = 200-10^6$) prepared by a collisional cooling cell.[4] The shift reported here would lead to this ice nanoparticle behavior, which smoothly converges to the bulk ice surface (the free OH frequency of the clean (0001) surface of hexagonal ice has been reported to be ~ 3695 cm^{-1}).[82,83] This surface OH frequency is consistent with the relaxation of the structural strains with increasing cluster size.[4]

4. Concluding Remarks

To analyze hydrogen bond network structures consisting of tens of water molecules, we measured IR spectra of moderately size-selected phenol$-(H_2O)_n$ ($n \leq \sim 50$) in the free OH stretching region. The observed spectra provided somewhat size-averaged information of the water clusters. The low-frequency shift of the free OH band with increasing cluster size was seen in the spectra. The detailed analyses with the aid of the DFT calculations indicated that the observed shift originates from the cooperativity of hydrogen bonds and the structural development from the highly strained 4-membered ring motif to the more relaxed 5- and 6-membered ring motifs. For further confirmation of the origin of the free OH frequency shift, spectral simulations including anharmonic frequency calculations for various isomer structures will be helpful.

This study shows the importance of a free OH frequency to probe water network structures. Because free OH bands are characteristic also of the bulk water surface,[82−85] it is hoped that detailed analyses of free OH frequencies are helpful to explore the correlation between the surface of bulk water and large-sized water clusters.

Acknowledgment. The authors are grateful to Professor N. Mikami in Tohoku University and Professor J.-L. Kuo in Nanyang Technological University for their helpful discussion. This study was supported by the Grant-in-Aid for Scientific Research (Project No. 19056001 on Priority Areas [477] "Molecular Science for Supra Functional Systems" from MEXT Japan, and Nos. 19205001 and 20·5015 from JSPS), and the Mitsubishi Foundation. K.M. is supported by JSPS Research Fellowships for Young Scientists. Most of the calculations were performed using supercomputing resources at Cyberscience Center, Tohoku University.

Supporting Information Available: Optimized structures of the clusters considered here and complete ref 71. This material is available free of charge via the Internet at http://pubs.acs.org.

References and Notes

(1) Eisenberg, D.; Kauzmann, W. *The structure and properties of water*; Oxford University press: Oxford, U.K., 1969.

(2) Maréchal, Y. *The hydrogen bond and the water molecule*; Elsevier: Oxford, U.K., 2007.

(3) Ludwig, R. *Angew. Chem., Int. Ed.* **2001**, *40*, 1808.

(4) Buch, V.; Bauerecker, S.; Devlin, J. P.; Buck, U.; Kazimirski, J. K. *Int. Rev. Phys. Chem.* **2004**, *23*, 375.

(5) Page, R. H.; Vernon, M. F.; Shen, Y. R.; Lee, Y. T. *Chem. Phys. Lett.* **1987**, *141*, 1.

(6) Pugliano, N.; Saykally, R. J. *Science* **1992**, *257*, 1937.

(7) Liu, K.; Cruzan, J. D.; Saykally, R. J. *Science* **1996**, *271*, 929.

(8) Liu, K.; Brown, M. G.; Carter, C.; Saykally, R. J.; Gregory, J. K.; Clary, D. C. *Nature* **1996**, *381*, 501.

(9) Buck, U.; Ettischer, I.; Melzer, M.; Buch, V.; Sadlej, J. *Phys. Rev. Lett.* **1998**, *80*, 2578.

(10) Buck, U.; Huisken, F. *Chem. Rev.* **2000**, *100*, 3863.

(11) Brudermann, J.; Buck, U.; Buch, V. *J. Phys. Chem. A* **2002**, *106*, 453.

(12) Steinbach, C.; Andersson, P.; Melzer, M.; Kazimirski, J. K.; Buck, U.; Buch, V. *Phys. Chem. Chem. Phys.* **2004**, *6*, 3320.

(13) Devlin, J. P.; Joyce, C.; Buch, V. *J. Phys. Chem. A* **2000**, *104*, 1974.

(14) Goss, L. M.; Sharpe, S. W.; Blake, T. A.; Vaida, V.; Brault, J. W. *J. Phys. Chem. A* **1999**, *103*, 8620.

(15) Steinbach, C.; Andersson, P.; Kazimirski, J. K.; Buck, U.; Buch, V.; Beu, T. A. *J. Phys. Chem. A* **2004**, *108*, 6165.

(16) Tsai, C. J.; Jordan, K. D. *J. Phys. Chem.* **1993**, *97*, 5208.

(17) Sremaniak, L. S.; Perera, L.; Berkowitz, M. L. *J. Chem. Phys.* **1996**, *105*, 3715.

(18) Wales, D. J.; Hodges, M. P. *Chem. Phys. Lett.* **1998**, *286*, 65.

(19) (a) Kazimirski, J. K.; Buch, V. *J. Phys. Chem. A* **2003**, *107*, 9762. (b) Buch, V. Data bank on ice and icy particles. http://www.fh.huji.ac.il/~viki/databank/IceParticles.html.

(20) Kabrede, H.; Hentschke, R. *J. Phys. Chem. B* **2003**, *107*, 3924.

(21) Fanourgakis, G. S.; Aprà, E.; Xantheas, S. S. *J. Chem. Phys.* **2004**, *121*, 2655.

(22) Fanourgakis, G. S.; Aprà, E.; de Jong, W. A.; Xantheas, S. S. *J. Chem. Phys.* **2005**, *122*, 134304.

(23) Lagutschenkov, A.; Fanourgakis, G. S.; Niedner-Schatteburg, G.; Xantheas, S. S. *J. Chem. Phys.* **2005**, *122*, 194310.

(24) Lenz, A.; Ojamäe, L. *Phys. Chem. Chem. Phys.* **2005**, *7*, 1905.

(25) Lenz, A.; Ojamäe, L. *J. Phys. Chem. A* **2006**, *110*, 13388.

(26) Lenz, A.; Ojamäe, L. *Chem. Phys. Lett.* **2006**, *418*, 361.

(27) Bandow, B.; Hartke, B. *J. Phys. Chem. A* **2006**, *110*, 5809.

(28) Kabrede, H. *Chem. Phys. Lett.* **2006**, *430*, 336.

(29) Takeuchi, H. *J. Chem. Inf. Model.* **2008**, *48*, 2226.

(30) Kazachenko, S.; Thakkar, A. J. *Chem. Phys. Lett.* **2009**, *476*, 120.

(31) Xantheas, S. S.; Aprà, E. *J. Chem. Phys.* **2004**, *120*, 823.

(32) Nguyen, Q. C.; Ong, Y. S.; Soh, H.; Kuo, J.-L. *J. Phys. Chem. A* **2008**, *112*, 6257.

(33) Maeda, S.; Ohno, K. *J. Phys. Chem. A* **2007**, *111*, 4527.

(34) Tharrington, A. N.; Jordan, K. D. *J. Phys. Chem. A* **2003**, *107*, 7380.

(35) Miyake, T.; Aida, M. *Chem. Phys. Lett.* **2006**, *427*, 215.

(36) Abe, H.; Mikami, N.; Ito, M. *J. Phys. Chem.* **1982**, *86*, 1768.

(37) Oikawa, A.; Abe, H.; Mikami, N.; Ito, M. *J. Phys. Chem.* **1983**, *87*, 5083.

(38) Fuke, K.; Kaya, K. *Chem. Phys. Lett.* **1983**, *94*, 97.

(39) Fuke, K.; Yoshiuchi, H.; Kaya, K.; Achiba, Y.; Sato, K.; Kimura, K. *Chem. Phys. Lett.* **1984**, *108*, 179.

(40) Lipert, R. J.; Colson, S. D. *Chem. Phys. Lett.* **1989**, *161*, 303.

(41) Stanley, R. J.; Castleman, A. W., Jr. *J. Chem. Phys.* **1991**, *94*, 7744.

(42) Hartland, G. V.; Henson, B. F.; Venturo, V. A.; Felker, P. M. *J. Phys. Chem.* **1992**, *96*, 1164.

(43) Tanabe, S.; Ebata, T.; Fujii, M.; Mikami, N. *Chem. Phys. Lett.* **1993**, *215*, 347.

(44) Bürgi, T.; Schütz, M.; Leutwyler, S. *J. Chem. Phys.* **1995**, *103*, 6350.

(45) Watanabe, T.; Ebata, T.; Tanabe, S.; Mikami, N. *J. Chem. Phys.* **1996**, *105*, 408.

(46) Ebata, T.; Fujii, A.; Mikami, N. *Int. Rev. Phys. Chem.* **1998**, *17*, 331.

(47) Jacoby, C.; Roth, W.; Schmitt, M.; Janzen, C.; Spangenberg, D.; Kleinermanns, K. *J. Phys. Chem. A* **1998**, *102*, 4471.

(48) Roth, W.; Schmitt, M.; Jacoby, C.; Spangenberg, D.; Janzen, C.; Kleinermanns, K. *Chem. Phys.* **1998**, *239*, 1.

(49) Janzen, C.; Spangenberg, D.; Roth, W.; Kleinermanns, K. *J. Chem. Phys.* **1999**, *110*, 9898.

(50) Lüchow, A.; Spangenberg, D.; Janzen, C.; Jansen, A.; Gerhards, M.; Kleinermanns, K. *Phys. Chem. Chem. Phys.* **2001**, *3*, 2771.

(51) Pribble, R. N.; Zwier, T. S. *Science* **1994**, *265*, 75.

(52) Gruenloh, C. J.; Carney, J. R.; Arrington, C. A.; Zwier, T. S.; Fredericks, S. Y.; Jordan, K. D. *Science* **1997**, *276*, 1678.

(53) Gruenloh, C. J.; Carney, J. R.; Hagemeister, F. C.; Arrington, C. A.; Zwier, T. S.; Fredericks, S. Y.; Wood, J. T., III; Jordan, K. D. *J. Chem. Phys.* **1998**, *109*, 6601.
(54) Gruenloh, C. J.; Carney, J. R.; Hagemeister, F. C.; Zwier, T. S.; Wood, J. T., III; Jordan, K. D. *J. Chem. Phys.* **2000**, *113*, 2290.
(55) Jiang, J. C.; Chang, J.-C.; Wang, B.-C.; Lin, S. H.; Lee, Y. T.; Chang, H.-C. *Chem. Phys. Lett.* **1998**, *289*, 373.
(56) Wang, Y.-S.; Jiang, J. C.; Cheng, C.-L.; Lin, S. H.; Lee, Y. T.; Chang, H.-C. *J. Chem. Phys.* **1997**, *107*, 9695.
(57) Miyazaki, M.; Fujii, A.; Ebata, T.; Mikami, N. *Science* **2004**, *304*, 1134.
(58) Shin, J.-W.; Hammer, N. I.; Diken, E. G.; Johnson, M. A.; Walters, R. S.; Jaeger, T. D.; Duncan, M. A.; Christie, R. A.; Jordan, K. D. *Science* **2004**, *304*, 1137.
(59) Wu, C.-C.; Lin, C.-K.; Chang, H.-C.; Jiang, J.-C.; Kuo, J.-L.; Klein, M. L. *J. Chem. Phys.* **2005**, *122*, 074315.
(60) Mizuse, K.; Fujii, A.; Mikami, N. *J. Chem. Phys.* **2007**, *126*, 231101.
(61) Schindler, T.; Berg, C.; Niedner-Schatteburg, G.; Bondybey, V. E. *Chem. Phys. Lett.* **1996**, *250*, 301.
(62) Sato, S.; Mikami, N. *J. Phys. Chem.* **1996**, *100*, 4765.
(63) Sawamura, T.; Fujii, A.; Sato, S.; Ebata, T.; Mikami, N. *J. Phys. Chem.* **1996**, *100*, 8131.
(64) Kleinermanns, K.; Janzen, C.; Spangenberg, D.; Gerhards, M. *J. Phys. Chem. A* **1999**, *103*, 5232.
(65) Shi, Z.; Ford, J. V.; Wei, S.; Castleman, A. W., Jr. *J. Chem. Phys.* **1993**, *99*, 8009.
(66) Braun, J. E.; Mehnert, T.; Neusser, H. J. *Int. J. Mass Spectrom.* **2000**, *203*, 1.
(67) (a) Becke, A. D. *Phys. Rev. A* **1988**, *38*, 3098. (b) Lee, C. T.; Yang, W. T.; Parr, R. G. *Phys. Rev. B* **1988**, *37*, 785. (c) Becke, A. D. *J. Chem. Phys.* **1993**, *98*, 5648.
(68) Although Kleinermanns et al. reported that the PhO• radical directly solvates the H_3O^+ moiety in the [phenol$-(H_2O)_4]^+$ (ref 64), cluster structures with a [PhO•H_3O^+] core did not survive during the geometry-optimization steps in our calculations of [phenol$-(H_2O)_{11}]^+$ and [phenol$-(H_2O)_{19}]^+$ because of the intracluster proton transfer.
(69) (a) Hodges, M. P.; Wales, D. J. *Chem. Phys. Lett.* **2000**, *324*, 279. (b) Wales, D. J.; Doye, J. P. K.; Dullweber, A.; Hodges, M. P.; Naumkin, F. Y.; Calvo, F.; Hernández-Rojas, J.; Middleton, T. F. The Cambridge cluster database. http://www-wales.ch.cam.ac.uk/CCD.html.
(70) Kuo, J.-L.; Klein, M. L. *J. Chem. Phys.* **2005**, *122*, 024516.
(71) Frisch, M. J.; et al. *Gaussian 03*, revision E.01; Gaussian, Inc.: Wallingford, CT, 2004.
(72) Flukiger, P.; Luthi, H. P.; Portmann, S.; Weber, J. *MOLEKEL 4.3*; Swiss Center for Scientific Computing: Manno, Switzerland, 2000−2002.
(73) Hobza, P.; Sponer, J.; Reschel, T. *J. Comput. Chem.* **1995**, *16*, 1315.
(74) Lynch, B. J.; Fast, P. L.; Harris, M.; Truhlar, D. G. *J. Phys. Chem. A* **2000**, *104*, 4811.
(75) Iikura, H.; Tsuneda, T.; Yanai, T.; Hirao, K. *J. Chem. Phys.* **2001**, *115*, 3410.
(76) Yanai, T.; Tew, D. P.; Handy, N. C. *Chem. Phys. Lett.* **2004**, *393*, 51.
(77) Grimme, S. *J. Comput. Chem.* **2006**, *27*, 1787.
(78) Jurecka, P.; Cerny, J.; Hobza, P.; Salahub, D. R. *J. Comput. Chem.* **2007**, *28*, 555.
(79) Zhao, Y.; Truhlar, D. G. *Theor. Chem. Acc.* **2008**, *120*, 215.
(80) Zhao, Y.; Truhlar, D. G. *Acc. Chem. Res.* **2008**, *41*, 157.
(81) Rauhut, G.; Pulay, P. *J. Phys. Chem.* **1995**, *99*, 3093.
(82) Wei, X.; Miranda, P. B.; Shen, Y. R. *Phys. Rev. Lett.* **2001**, *86*, 1554.
(83) Wei, X.; Miranda, P. B.; Zhang, C.; Shen, Y. R. *Phys. Rev. B* **2002**, *66*, 085401.
(84) Du, Q.; Superfine, R.; Freysz, E.; Shen, Y. R. *Phys. Rev. Lett.* **1993**, *70*, 2313.
(85) Tarbuck, T. L.; Ota, S. T.; Richmond, G. L. *J. Am. Chem. Soc.* **2006**, *128*, 14519.

JP9061187